Microscopy and spectroscopy on model catalysts in gas environments

Wenzel, S.

Chapter 4

Gold Oxide Formation on TiO_2/Au(111) during CO Oxidation

4.1 Introduction

Whereas conventional power plants can be turned on and off as needed, the energy output of wind and solar plants varies with the weather and the time of day. Therefore, the transition to sustainable energy sources requires the development of efficient energy-storage methods. A viable option is to store the energy in the form of chemicals such as methanol. As a liquid at room temperature [71], methanol is simple to store and it is biodegradable [70]. In comparison to other hydrocarbons, methanol has the highest hydrogen-to-carbon ratio. The energy stored in the form of methanol can be harvested by converting it to hydrogen via methanol steam reforming [72,76]. However, for the use in fuel cells this hydrogen needs to be free from carbon monoxide, a byproduct of methanol steam reforming, to prevent poisoning of the fuel-cell anode [74]. In Section 3.1 of this thesis we mention the strong research effort to improve the selectivity of methanol steam reforming catalysts towards CO_2 instead of CO. An alternative solution is removing the traces of CO over a second catalyst via preferential CO oxidation, which takes place in the hydrogen environment without oxidation of the H_2:

$$2\ CO + O_2 \rightarrow 2\ CO_2 \tag{4.1}$$

$$2\ H_2 + O_2 \not\rightarrow 2\ H_2O \tag{4.2}$$

Compared to conventional CO oxidation catalysts such as platinum and palladium, gold-based catalysts are more suited for this application, since they are more selective for the oxidation of CO instead of H_2 at low temperatures [131–133]. Gold-based catalysts have shown CO oxidation activity at temperatures as low as room temperature [134]. They are thus additionally interesting for improving the 3-way car catalyst, which is currently not efficiently oxidizing CO during the cold start-up of the car [135]. There has been research into the catalytic activity of gold nanoparticles deposited on oxide supports for more than 30 years [136–141]. Inverse model catalysts of oxide particles on metal single crystals are widely applied as well due to the ease of controlled preparation and application of surface-science techniques, especially in ultra-high vacuum [29,141,142]. On Au(111) single crystals various oxide nanoparticles have been prepared. Among these are CeO_2 [143], MoO_3 [144], MgO [145], CoO [146], Fe_2O_3 [147], and TiO_2 [148]. However, inverse model catalysts on gold single crystals are not only a useful research tool but can also show even higher CO oxidation activities than their non-inverse counterparts as suggested by Palomino et al. [34]. In their study, TiO_2/Au(111) showed the highest activity of all tested catalysts. For inverted as well as non-inverted catalysts it is clear that the active site lies in the interface region between support and particles [149–151] and metal-support interactions have been observed [34,152,153]. However, the exact oxidation state of gold during the reaction remains under debate. The oxidation of gold is believed to not be possible from

molecular oxygen [154–156] and more specifically under CO oxidation conditions [157]. There is evidence that a gold oxide prepared with ozone would be less active than metallic gold [158]. However, other work has suggested that oxidized gold is the active species during CO oxidation [159,160]. Additionally, there is evidence that water can promote the CO oxidation reaction [161–163] and could even make the oxide support unnecessary [164].
The challenges in investigating the presence of a gold oxide with spectroscopy techniques are the low signals stemming from small amounts of surface oxides as well as the influence of exposing the sample to air and thus water between the reaction and the characterization as is necessary in many laboratories. However, crystalline surface oxides can be detected via atomically resolved microscopy as well [96,165–167].
Our in situ scanning tunneling microscope allows for the imaging of the support and the full inverse model catalyst under reaction conditions. In this chapter we present evidence for the presence of a gold oxide on Au(111) after exposure to oxygen (Section 4.3.1) and differentiate between the influence of the water background in the reactor (Section 4.3.2), the CO in the reaction mixture (Section 4.3.3), the TiO_2 nanoparticles (Section 4.3.4), and finally contaminants on the gold substrate (Section 4.3.5). In the outlook in Section 4.4 we give a suggestion on how the presence of the gold oxide on this model catalyst could be confirmed using spectroscopy.

4.2 Materials and Methods

4.2.1 Sample Preparation

The Au(111) single crystal was purchased from SPL and prepared with cycles of argon ion sputtering at 1 kV to 1.4 kV acceleration voltage and annealing to between 800 K and 850 K in UHV. Whenever carbon particles were visible in the STM, the crystal was additionally annealed in $1{\cdot}10^{-6}$ mbar of O_2 to between 750 K and 800 K until the carbon was removed. This was followed by at least ten cycles without annealing in oxygen before running an experiment.
For the preparation of the TiO_2/Au(111) model catalyst titanium was deposited onto the clean, metallic Au(111) using an e-beam evaporator from Oxford Applied Research. The deposition was performed in an oxygen background of $1{\cdot}10^{-6}$ mbar at room temperature. Subsequently the crystal was annealed to 850 K in $5{\cdot}10^{-6}$ mbar of O_2 for 20 min and cooled down in the same oxygen pressure until below 500 K. To exclude any influence from titanium residue or alloying of titanium with gold the experiments in Sections 4.3.1 to 4.3.3 and 4.3.5 were performed on a crystal that had not been exposed to titanium whereas another crystal was used solely for the experiments on TiO_2/Au(111).

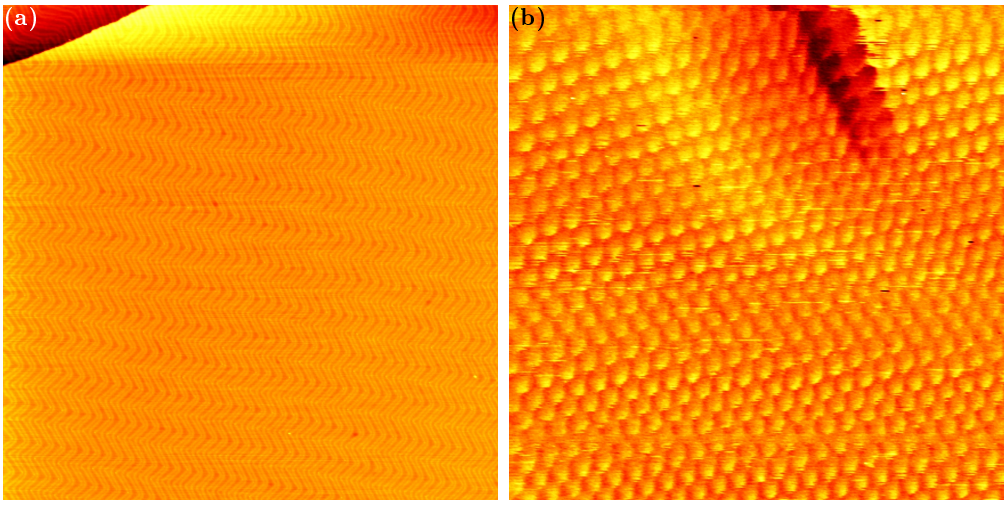

Figure 4.1: (a) 300 nm x 300 nm STM image of the as-prepared Au(111) surface and (b) 10 nm x 10 nm STM image of the same surface with atomic resolution. Both images are taken in UHV at room temperature with − 1 V and 50 pA.

4.2.2 The ReactorSTM

As described in more detail in Section 3.2.1 and in Ref. [44], the ReactorSTM setup allows for scanning tunneling microscopy in ultra-high vacuum as well as in up to 6 bar of gases and at up to 600 K. Without leaving the vacuum chamber the sample can be moved between preparation, STM, LEED/Auger, and XPS.

4.2.3 Gases

The amount of water in our gas system was measured for 1 bar Ar and 1 bar O_2 with a result on the order of 1 mbar of water. Section 3.2.2 describes the measurement process and that the water background in our system is likely independent of which gases are used. In the following we have used Ar 5.0 from Westfalen [97], O_2 5.0 from Westfalen [168], and CO 4.7 from Air Liquide [169]. The CO contains less than 5 ppm of O_2.

4.3 Results and Discussion

4.3.1 Gold Oxide on Au(111)

Figure 4.1(a) shows an overview of the as-prepared Au(111) surface with the well-known herringbone reconstruction visible as brighter lines with straight sections as well as so-called elbows. The hexagonal unit cell of Au(111) can be seen in the zoomed-in image

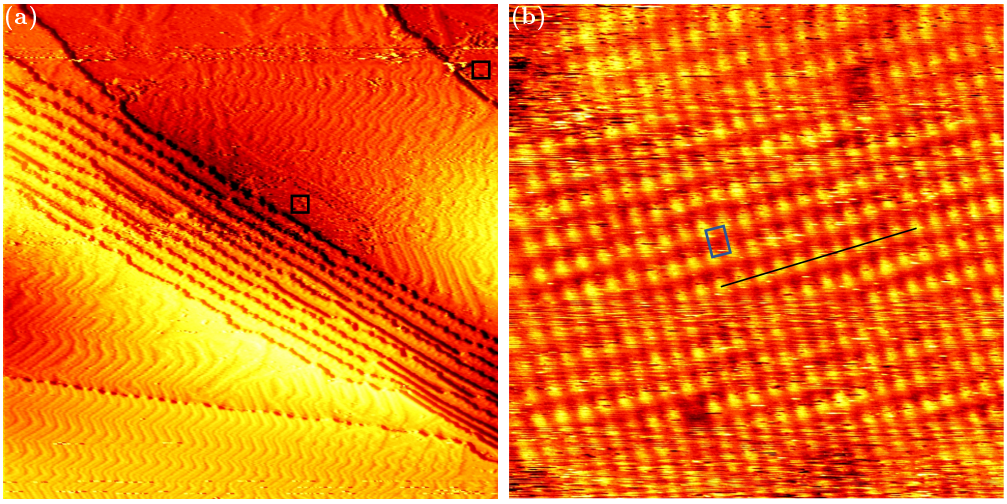

Figure 4.2: (a) 300 nm x 300 nm STM image of Au(111) after exposure to 0.8 bar O_2 at room temperature for 1 h. For better visibility of the structure next to the step edges (marked with black squares) the image is merged with its derivative in a ratio of 1:15. (b) 10 nm x 10 nm STM image of the newly formed structure indicating the rectangular unit cell in blue. Following the black line deviations from the unit cell can be seen, which are discussed in the supplemental information (Section 4.5.2). Both images are taken in UHV at room temperature with − 1 V and 50 pA.

in Figure 4.1(b) including part of a herringbone in the upper right corner.
After exposing this surface to 0.8 bar O_2 at room temperature for 1 h, the herringbone is still present on most part of the terraces (see Figure 4.2(a)). Additionally, islands of another structure with a height of about (0.09 ± 0.02) nm are visible on step edges as marked with black squares. An area as large as the square (10 nm x 10 nm) is shown close up in Figure 4.2(b). Averaging over tens of STM images the size of the unit cell is determined to be (0.50 ± 0.07) nm in the longer direction and (0.37 ± 0.03) nm in the shorter direction with the standard deviations as error. As shown in the supplemental information (Section 4.5.1), the same unit cell is observed when the Au(111) surface is exposed to atomic oxygen before the exposure to atmospheric oxygen pressures. Additionally, it has been observed in STM by Min et al. after exposing Au(111) to ozone (see Figure 9 in Ref. [165]). Overall, this allows for identifying the islands as surface gold oxide. When using atomic oxygen, the oxide can also grow on the terraces (see Figure 4.12(b) in the supplemental information) as opposed to only at step edges as in Figure 4.2. This allows for the observation of three different orientations of the oxide unit cell as is to be expected for a rectangular structure on top of the hexagonal Au(111) substrate. The presence of the unit cell seen in STM is additionally evidenced by a

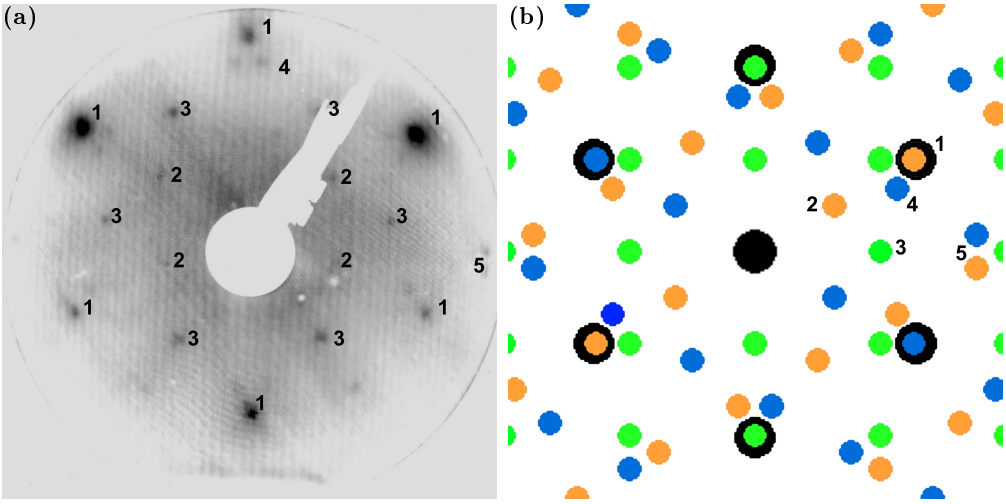

Figure 4.3: (a) LEED image taken of Au(111) after O_2 exposure (78 eV electron energy). Measurement done by Dajo Boden, Leiden Institute of Chemistry. (b) Simulated LEED image based on the unit cell measured in STM including the Au(111) substrate in black and the three different possible orientations of the oxide overlayer in blue, orange, and green. Corresponding spots in (a) and (b) are marked with numbers 1 to 5. The simulated LEED image is made using LEEDpat [170].

LEED measurement as seen in Figure 4.3(a). This is in agreement with the simulated LEED image of the unit cell in Figure 4.3(b) and shows all three different orientations. Additional details on the unit cell of the gold oxide and a model for the structure of the oxide is given in the supplemental information (Section 4.5.2).
Although we can detect the presence of oxygen on the surface with XPS (data not shown), the surface sensitivity of our lab setup is not large enough to distinguish between adsorbed atomic oxygen and gold oxide (for details see Section 4.4). Note that in order to observe the unit cell in LEED and the presence of oxygen in XPS a higher coverage of the gold oxide is needed, which can only be achieved on contaminated samples in the presence of CO as described in Section 4.3.5.

4.3.2 The Role of Water

The theoretical dissociation barriers of O_2 on the Au(111) terraces of 2.23 eV and on the Au(111) step edge of 1.16 eV [171] suggest that O_2 dissociation even on the step edge is unlikely in pure O_2. To test whether water could deliver the necessary atomic oxygen, the as-prepared Au(111) was exposed to 0.8 bar argon for 1 h and thus the

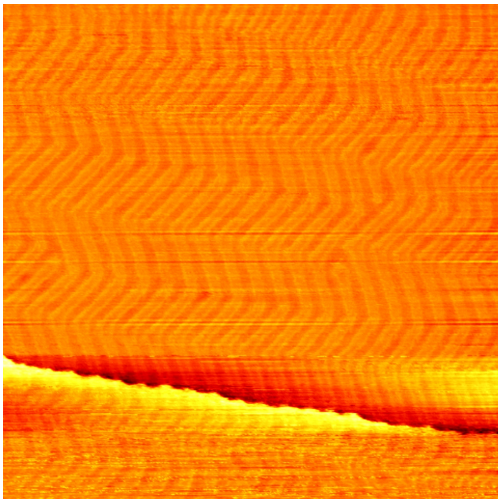

Figure 4.4: 150 nm x 150 nm STM image of the as-prepared Au(111) surface after 1 h in 0.8 bar argon, containing roughly 1 mbar of water, at room temperature. The image is taken in UHV at room temperature with − 1 V and 50 pA.

same amount of water as was present during the O_2 exposure. No oxide islands could be found after this water exposure and the herringbone reconstruction stayed intact as can be seen in Figure 4.4. Water alone does thus not cause the formation of gold oxide, which can be understood on the hands of theoretical dissociation barriers as well: Whereas the dissociation barrier of H_2O is somewhat lower than the barrier of O_2 on the terraces with 1.80 eV [172], it is slightly higher than the barrier of O_2 at the step edges with 1.33 eV [173]. However, Liu et al. [174] have shown that the presence of water reduces the dissociation barrier of oxygen on the steps of Au(111). With two water molecules per oxygen molecule the barrier is already reduced to 0.54 eV and with a larger amount of water molecules the barrier can be as low as 0.15 eV. Given that our gas mixtures contain on the order of 1 mbar of water, it is probable that this water-assisted dissociation of molecular oxygen on the Au(111) steps supplies the first atomic oxygen from which the gold oxide can start growing. However, only one island per 320 nm x 320 nm is present on average after 1 h of oxygen exposure showing that this is still a rare event. Once an island of gold oxide exists, it is believed to be able to dissociate more O_2 from the gas phase [165,175] allowing the islands to keep growing away from the step. In situ images of the formation of gold oxide are shown in the supplemental information (Section 4.5.3).

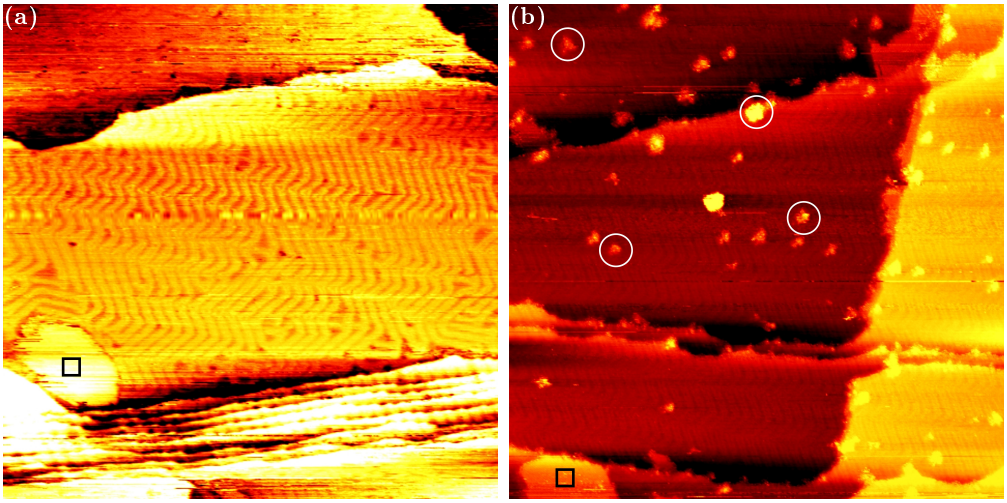

Figure 4.5: 300 nm x 300 nm STM images of Au(111) (a) after 1 h in 1 bar of 4 O_2 + 1 CO and (b) after 1 h in 0.2 bar CO, respectively. The images are taken in UHV at room temperature with (a) − 1 V and (b) − 1.5 V, and 50 pA. Black squares mark islands of gold oxide. White circles mark structures which likely consist of carbon.

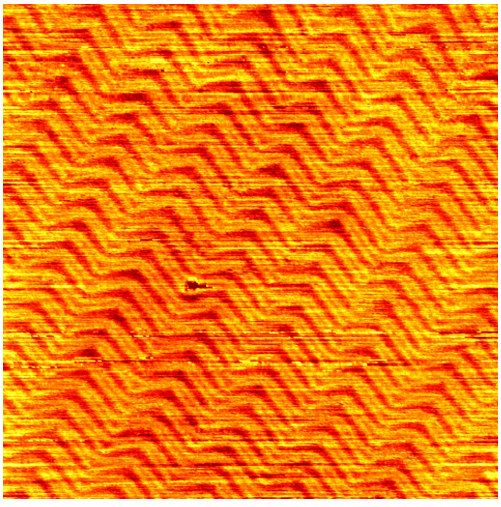

Figure 4.6: 150 nm x 150 nm STM image of Au(111) after 88 min of exposure to increasing CO pressure followed by 13 min at 1 bar. The image is taken in 1 bar CO at room temperature with − 1 V and 50 pA. Horizontal lines caused by a disturbed STM tip have been removed.

4.3.3 The Influence of CO

Figures 4.5(a) and (b) show Au(111) after exposure to CO oxidation conditions (1 bar 4 O_2 + 1 CO) and 0.2 bar CO for 1 h, respectively. Comparing several images of these measurements with the images of the sample exposed to oxygen only (see Figure 4.2(a)), the number and size of the gold oxide islands are comparable. This indicates no promoting or inhibiting influence by the CO on the oxidation of clean Au(111). There is no evidence in the literature that CO itself dissociates on Au(111) and adsorption is only possible at the steps [176–178]. However, after exposure to only CO, additional structures with roughly round shapes can be observed as bright spots on the terraces in Figure 4.5(b) marked with white circles. As discussed in more detail in the supplemental information (Section 4.5.4), these are likely carbon structures, but whether they stem from the CO itself or from contaminants in the gas bottle is unclear. As most of these structures are observed on the terraces and not in proximity to the oxide islands, any relevance for the formation of the oxide can be deemed unlikely. As suggested above (see Section 4.3.2), the first O_2 dissociation initiating the growth of an oxide island is a rare event. Therefore, it is reasonable that the 10^{-3} mbar range of O_2 present in 0.2 bar CO (see Section 4.2.3) is sufficient to produce a roughly comparable number of islands as in 0.8 bar O_2. However, it could be expected that the self-catalyzed growth of existing islands from O_2 would proceed more slowly here. We cannot find conclusive evidence for this when comparing average sizes of islands for multiple images after exposure to the different gas compositions. Thus it is likely that, in the pressure range studied here, the amount of O_2 in the gas phase is not the limiting factor for the growth speed.

Figure 4.5(b) additionally clearly shows that the herringbone reconstruction is still intact after CO exposure. This is further confirmed in Figure 4.6 showing an in situ image of the Au(111) in 1 bar CO after 12.7 min at this pressure with the herringbone intact. This contradicts Piccolo et al. [179] observing a complete lifting of the herringbone in 333 mbar CO, which is not reversible when returning to UHV. We comment further on this in Section 4.3.5.

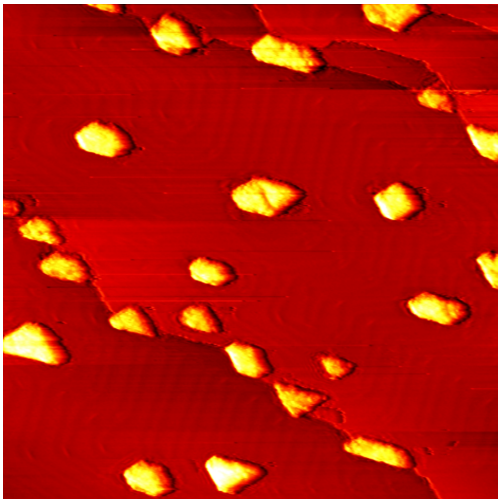

Figure 4.7: 110 nm x 110 nm STM image of the as-prepared TiO_2/Au(111) taken in UHV at room temperature with + 3 V and 50 pA. In order for the particles and the herringbone to be visible simultaneously the image was flattened and merged with its derivative.

4.3.4 Gold Oxide on TiO_2/Au(111)

Figures 4.7 and 4.8(a) show the as-prepared TiO_2/Au(111) model catalyst. The nanoparticles are roughly between 5 nm and 15 nm wide and show an apparent height between 0.6 nm and 1.9 nm in the STM. Triangular, hexagonal, and more elongated shapes can be recognized suggesting a crystalline structure. In general, the TiO_2 nanoparticles are in agreement with those prepared by Biener et al. [148]. A more detailed analysis can be found in Ref. [180].
In Figure 4.8 the as-prepared TiO_2/Au(111) surface is compared to the same surface after exposure to O_2, CO oxidation conditions, and CO, respectively. Under all conditions, islands of gold oxide are formed at step edges as marked with a black square. The amount of gold oxide is comparable to the amount seen when exposing only the Au(111) substrate as presented in Sections 4.3.1 and 4.3.3. Specifically, no oxide islands are observed on the terraces despite the presence of the TiO_2 nanoparticles suggesting that no spillover of atomic oxygen from the titania to the gold substrate takes place. Studies on TiO_2 single crystals suggest that dissociation of molecular oxygen is possible at oxygen vacancies in the titania at room temperature [181]. Additionally, the dissociation is increasingly more likely with higher vacancy density [182]. If oxygen dissociation takes place on the titania in our case, the resulting oxygen atoms might thus rather remain on the nanoparticles curing vacancies instead of spilling over to the gold substrate.

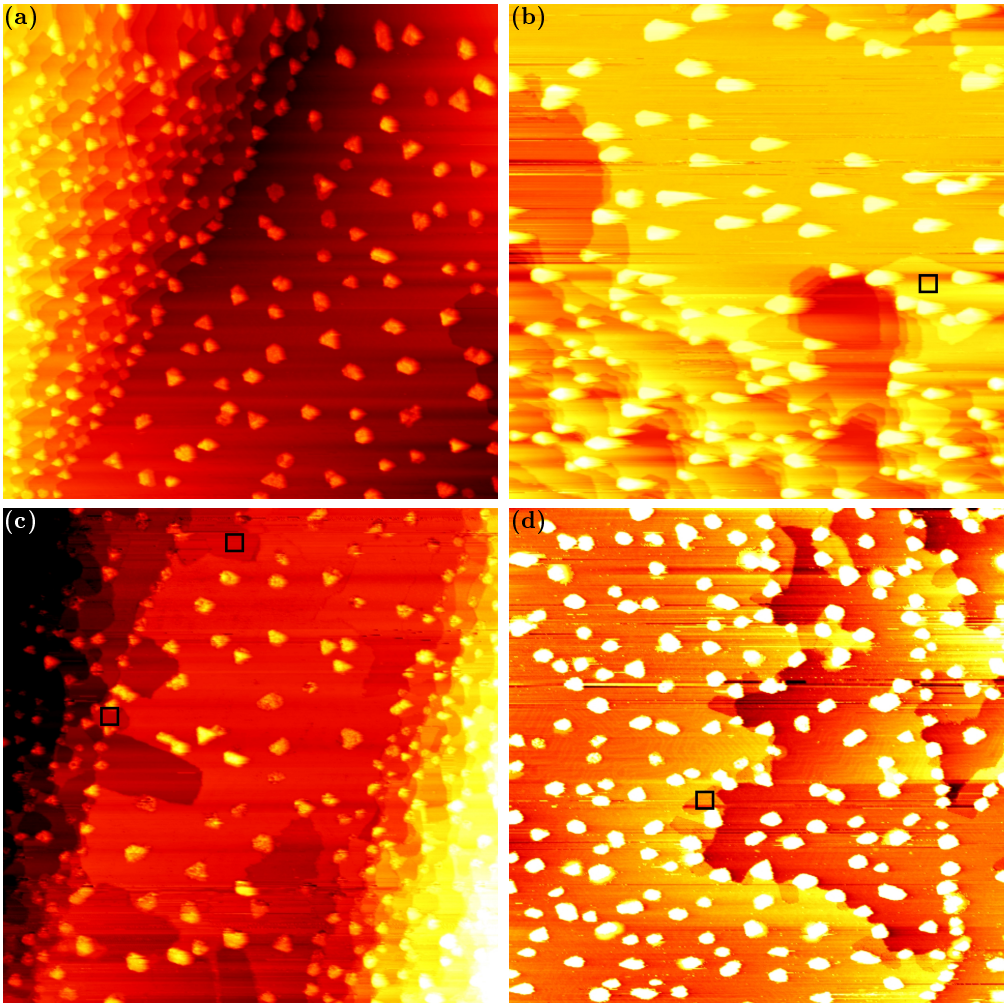

Figure 4.8: 300 nm x 300 nm STM images of TiO_2/Au(111) (a) as-prepared, (b) after 1 h in 0.8 bar O_2, (c) after 1 h in 1 bar of 4 O_2 + 1 CO, and (d) after 1 h in 0.2 bar CO, respectively. All images are taken in UHV at room temperature with + 3 V and 50 pA. Black squares mark islands of gold oxide. The size of the squares corresponds to the size of the atomic-resolution image of the gold oxide in Figure 4.2(b).

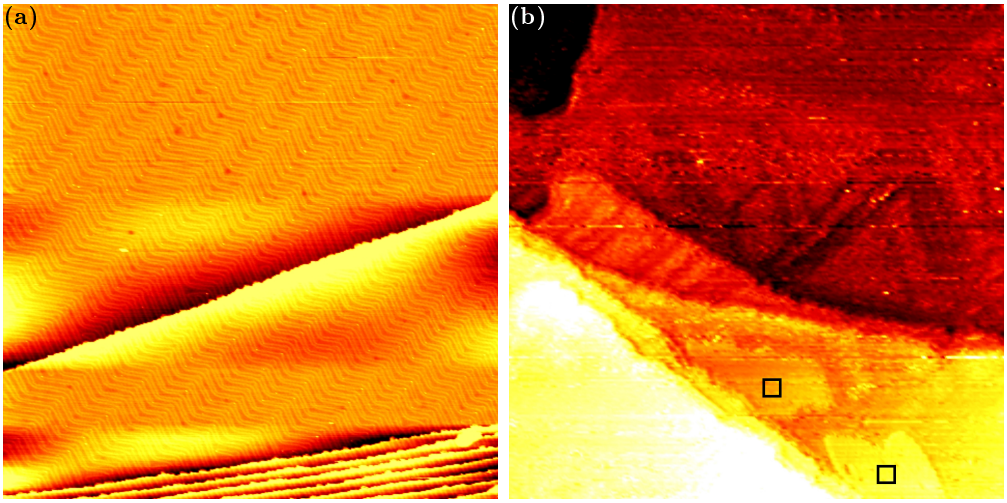

Figure 4.9: 300 nm x 300 nm STM images of contaminated Au(111) (a) as-prepared and (b) after 1 h in 0.8 bar O_2. The images are taken in UHV at room temperature with (a) − 2 V and (b) − 1.5 V, and 50 pA. Black squares mark islands of gold oxide.

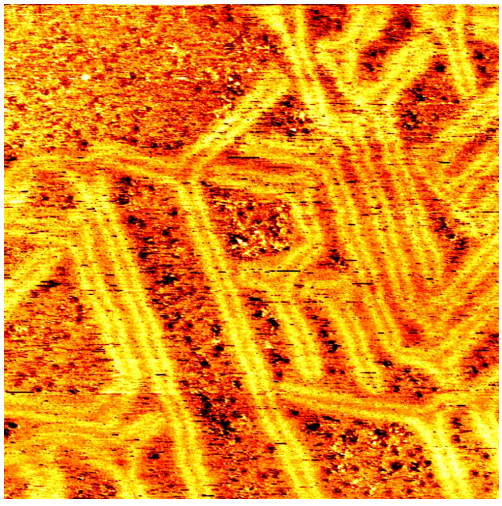

Figure 4.10: 120 nm x 120 nm STM image of a terrace of contaminated Au(111) after 1 h in 0.8 bar O_2. The image is taken in UHV at room temperature with + 1.5 V and 50 pA.

4.3.5 Sensitivity to the Cleanliness of the Substrate

Figure 4.9(a) shows the Au(111) substrate in a contaminated state, which is present when a newly purchased single crystal has been submitted to less cleaning cycles than needed to fully clean the crystal (as in Figure 4.1). Bright spots on elbows of the herringbone as well as darker spots in between the reconstruction lines are visible on the contaminated gold. Carbon as well as other metals are typical candidates for these contaminants. However, the amount present on the surface is not sufficient to allow for a spectroscopic characterization with the methods available in the ReactorSTM setup (XPS and AES). Additionally, this means that the amount of contamination cannot be quantified precisely and repeated preparation of this surface will lead to deviations in the amount and nature of contaminants present. However, general trends can be observed compared to the clean gold when exposing a contaminated surface to the same gas environments.
Figure 4.9(b) shows that the exposure to 0.8 bar O_2 leads to a comparable number and size of gold oxide islands as on the clean gold in Figure 4.2(a). However, most of the terrace does not show the herringbone reconstruction anymore. This can be seen more clearly in Figure 4.10. Areas which appear amorphous (meaning that no atomic resolution could be achieved) are separated by single lines of herringbone. This suggests a mobility of the surface gold atoms during O_2 exposure. A restructuring of Au(111) can be expected from literature under exposure to atomic oxygen (or ozone) [183,184] as well as in O_2 at elevated temperatures [185–187]. As the amount of gold oxide is comparable to the case of clean gold, the presence of significantly more atomic oxygen is unlikely. It is more probable that the contaminants promote the restructuring by O_2 similar to the effect of an elevated temperature. For the case of oxygen exposure we have not been able to achieve the necessary resolution in situ to determine whether the herringbone on clean gold is lifted as well but recovers when returning to UHV. Thus it remains unclear whether the contaminants are the cause of the changes on the terrace or whether they only prevent them from being reversible.
When CO is present in the gas mixture (Figure 4.11(a) and (b)), the number of gold oxide islands can be higher than on clean gold and oxide islands which are not connected to a step edge are observed. This suggests that the contaminants form sites on the step edges as well as on the terraces where oxygen can dissociate aided by CO (and possibly by water) more readily than on clean gold. It is possible that these dissociation sites are the contaminants themselves, low-coordinated Au atoms caused by the contaminant, or a combination of both. Other metals are known to dissociate O_2 directly [156]. However, density functional theory calculations suggest that the presence of CO hampers the O_2 dissociation on Pd and Pt single crystals [188,189]. Silver is the most likely bulk contaminant in the gold single crystal according to the analysis provided by

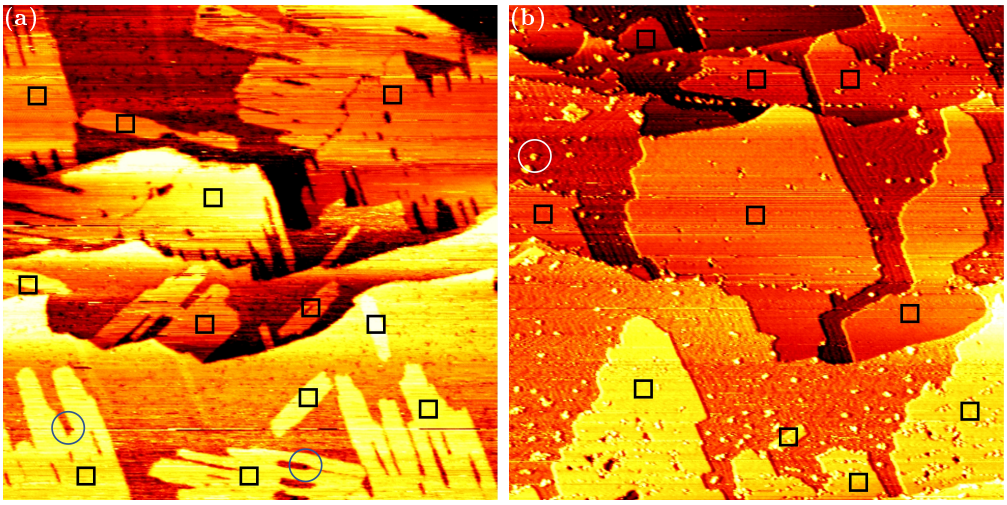

Figure 4.11: 300 nm x 300 nm STM images of contaminated Au(111) (a) after 1 h in 1 bar of 4 O_2 + 1 CO and (b) after 1 h in 0.2 bar CO, respectively. The images are taken in UHV at room temperature with (a) − 1.5 V and (b) − 1 V, and 50 pA. Black squares mark islands of gold oxide and blue circles mark a certain type of contaminants that blocks the growth of islands. A white circle marks a structure which likely consist of carbon. For better visibility of the herringbone on the terraces the image in (b) is merged with its derivative in a ratio of 1:2.

the supplier. Although Ag(111) is inert for O_2 dissociation, low-coordinated Ag sites might easily split O_2 [156]. Carbon as a possible contaminant is a less likely candidate for O_2 dissociation [190,191]. As described in detail in the supplemental information (Section 4.5.4), we identify carbon structures on the surface after CO exposure (see also area marked with a white circle in Figure 4.11(b)). That many of these areas are observed on the terraces without gold oxide islands connected to them confirms that carbon is likely not responsible for the promotion of gold oxide formation observed in Figure 4.11(a) and (b).

We do not only observe more gold oxide islands, but a single island can also grow larger than on clean gold during the same exposure time. As we identify the O_2 dissociation on already oxidized gold as responsible for this in Section 4.3.2, we have to conclude here that the dissociation promoted by contaminants is more efficient than the self-catalyzed growth or that the latter is promoted by the contaminants as well.

In Figure 4.11(a) blue circles mark positions where it can be seen that contaminants, possibly of a different nature, are able to block the growth of the oxide islands as well, which leads to more irregular shapes. As a common contaminant that is known to form pinning sites on Au(111) and does not promote O_2 dissociation, it is likely that this

contaminant is carbon.
Apart from the gold oxide islands, the terraces of the gold substrate are influenced as well. Similar to after oxygen exposure, a lifting of the herringbone is observed with only a few lines left after exposure to the reaction mixture. As this suggests that the surface atoms of gold are mobile during the exposure, it is possible that it aids in the formation of sites of low-coordinated gold atoms and/or contaminants where stronger O_2 dissociation takes place. As the herringbone is not lifted after exposure to pure CO (Figure 4.11(b)), the more complete lifting of the herringbone in the mixture (Figure 4.11(a)) compared to O_2 exposure (Figure 4.9(b)) cannot be interpreted as a sign of a promotion by CO. However, as explained above, a deviation in the exact amount of contaminants could likely cause the more complete lifting in the mixture. Although the contaminants seem to promote the restructuring of the herringbone in O_2, they are not sufficient to lead to a loss of herringbone in CO in our case. Thus, the presence of the type of contaminants observed here cannot explain the discrepancy stated in Section 4.3.3 where no lifting of the herringbone in CO is observed despite evidence to the contrary in the literature [179].

4.4 Conclusions and Outlook

We have presented evidence for the formation of surface gold oxide on TiO_2/Au(111) model catalysts under exposure to O_2, CO, or a mixture of both at atmospheric pressures. The formation is likely enabled by water in all gas mixtures and can be strongly promoted by CO when contaminants are present on the Au(111) substrate. Taking into account that under industrial conditions the same or more water is present and the gold is less pure, it is reasonable to assume that gold oxide could be formed during the reaction on a realistic catalyst. As we do not see any influence of titania on the gold oxide formation, it is unlikely that the transfer of atomic oxygen from one to the other is a possible step in the CO oxidation mechanism. Assuming that our conclusion about the role of water is correct, our observations cannot confirm that titania and water have interchangeable roles as suggested in Ref. [164]. Additional evidence for the role of water in the formation of gold oxide should be collected by exposing all as-prepared surfaces studied here to dried gases. Reducing the water content in our gas delivery system has not been successful so far for technical reasons. Although we have observed the presence of oxygen in XPS and the crystalline structure in STM which has the same unit cell as gold oxide, this does not yet confirm that gold is in a non-metallic oxidation state during the reaction as proposed in Ref. [159]. The presence of oxidized gold in a spectroscopic gold signal would be the only direct evidence that an oxidized gold species is present during the reaction and thus

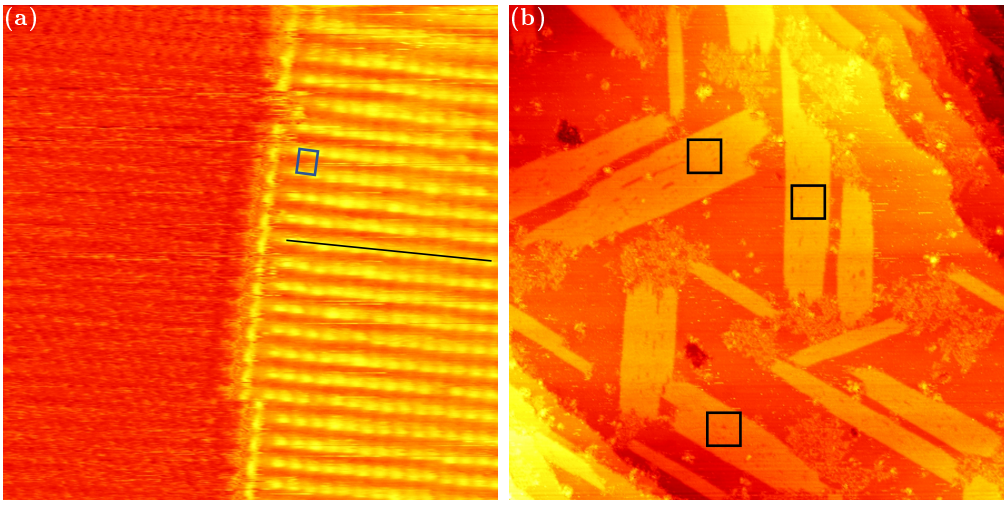

Figure 4.12: (a) 10 nm x 10 nm STM image of O/Au(111) prepared using a hot tungsten filament in oxygen background and subsequently exposed to 1 bar O_2 for several hours. The rectangular unit cell of gold oxide is marked in blue. Following the black line, deviations from the unit cell can be seen, which are discussed in Section 4.5.2. (b) 140 nm x 140 nm STM image of the same surface showing the three possible orientations of gold oxide islands marked with black squares of 10 nm x 10 nm. The images are taken in UHV at room temperature with (a) + 0.3 V and 140 pA, and (b) + 1 V and 80 pA.

confirm that a real gold oxide and not just an adsorbed oxygen species has been observed here. As the coverage of the surface oxide is limited to less than a monolayer, a highly surface-sensitive measurement is needed to distinguish the oxidized gold peak from the bulk metallic gold peak stemming from the substrate. This could be achieved using synchrotron XPS. As atomic oxygen or ozone is necessary to form the oxide in UHV, studying its formation under CO oxidation conditions will require near-ambient pressure XPS.

4.5 Supplemental Information

4.5.1 Gold Oxide Formed from Atomic Oxygen

For comparison to the surfaces studied above, one gold sample was oxidized in O_2 after depositing a seed of atomic oxygen. In this case a tungsten filament facing the surface was turned on in an oxygen background on the order of $1{\cdot}10^{-5}$ mbar for 75 min before exposure to atmospheric pressures of O_2. As shown in Figure 4.12(a), this leads to the formation of the same structure as described in Section 4.3.1 as evidenced by the same

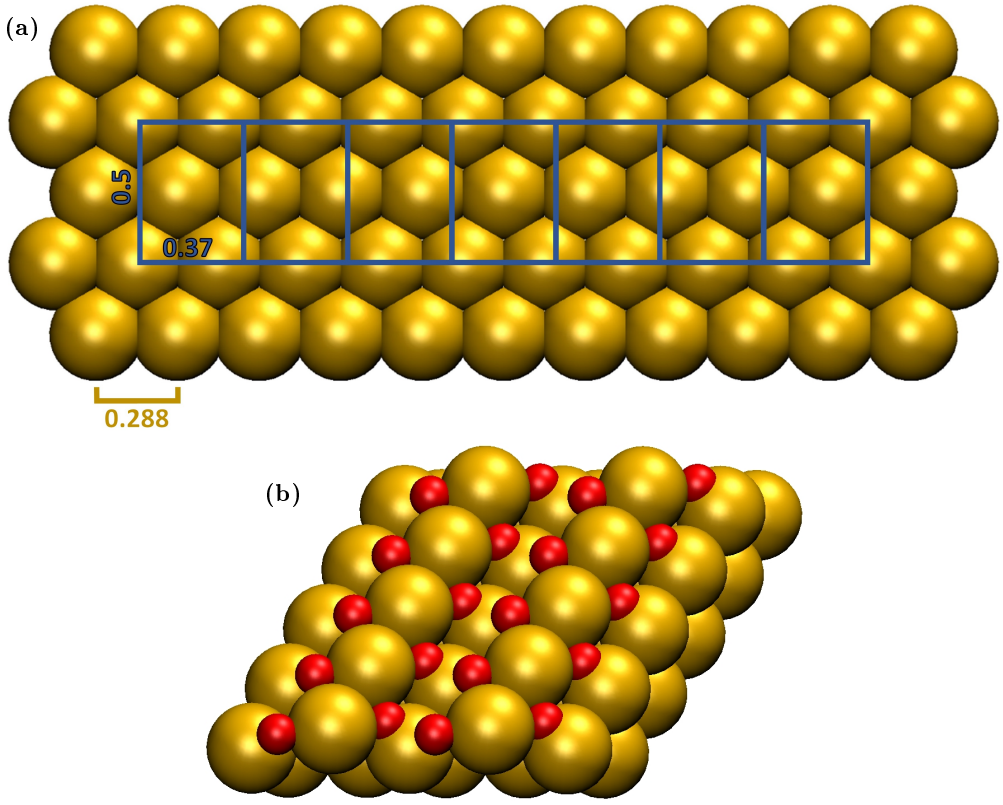

Figure 4.13: (a) Comparison of the measured gold oxide unit cell to the unit cell of the Au(111) substrate. Lengths in nm. (b) Proposed structure of the surface gold oxide showing gold atoms in gold and oxygen atoms in red.

rectangular unit cell. In the larger overview in Figure 4.12(b), it can be seen that the use of an atomic oxygen seed allows for the growth of gold oxide islands which are not connected to a step. In this case, the three possible orientations of the rectangular gold oxide unit cell on top of the hexagonal unit cell of the gold substrate can be seen.

4.5.2 Structure of the Gold Oxide

On a larger scale, the crystalline gold oxide shows slight deviations from the unit cell measured in Section 4.3.1: When following the black lines drawn in Figures 4.2(b) and 4.12(a) parallel to the short side of the gold oxide unit cell, it can be seen that the brightest spots are not always centered on this line but some appear slightly above or below the line. This can be explained by comparing the measured gold oxide unit cell to the unit cell of the Au(111) substrate as is done in Figure 4.13(a). The long side

of the measured oxide unit cell of (0.50 ± 0.07) nm agrees with the shortest distance between two gold atoms in the vertical direction in 4.13(a). However, the short side of the measured oxide unit cell of (0.37 ± 0.03) nm does not match with the substrate unit cell. This indicates that the actual unit cell of the gold oxide including the Au(111) substrate is larger and contains the measured 0.5 nm x 0.37 nm unit cell multiple times. Figure 4.13(a) shows that a reasonable agreement with the substrate can be achieved when the actual gold oxide unit cell is at least seven times as long as the measured gold oxide unit cell.
Despite the actual unit cell not being known unambiguously, we want to offer a rough idea of the structure that the gold oxide could have. Inspired by similar surface oxide structures on Pt(111) [192,193] this structure is given in Figure 4.13(b). Rows of gold atoms (gold) are lifted out of the surface with oxygen atoms (red) on either side.

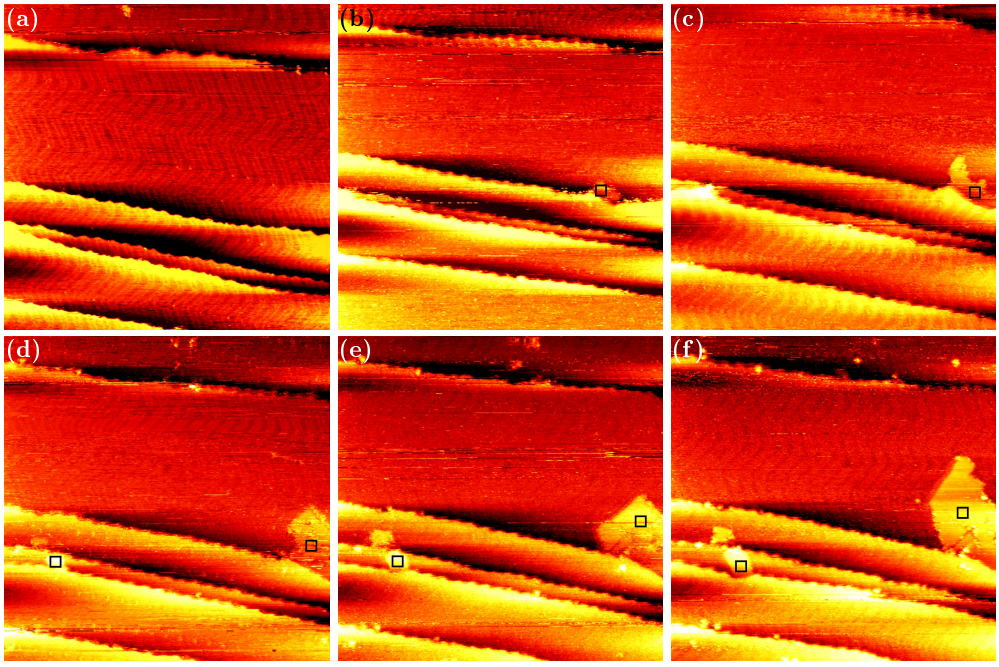

Figure 4.14: 160 nm x 160 nm STM images of Au(111) in 0.2 bar CO at (a) 0 min, (b) 2.2 min, (c) 4.8 min, (d) 13.1 min, (e) 17.5 min, and (f) 24.1 min since the start of the exposure. All images are taken with − 1 V and 50 pA. No more than five horizontal lines were removed from each of the images. A global plane filter which does not reflect the step edges correctly was chosen because it allows for a clearer visibility of the herringbone as well as the gold oxide island on the largest terrace in the image. Islands of gold oxide are marked with a black square of 5 nm x 5 nm.

4.5.3 Formation of the Gold Oxide

Figure 4.14 shows the formation of a gold oxide island on Au(111) in 0.2 bar CO. Upon introducing the gas to the reactor the gold oxide (marked with black squares) starts to grow almost immediately, starting from the step edge. The island on the lower right grows primarily in the direction towards the upper left corner of the images whereas it does not grow significantly in the orthogonal direction anymore from (d) on. In most cases where no step edges or nanoparticles limit the available space, we observe gold oxide islands which are longer parallel to the long side of the rectangular unit cell, which indicates a preferred growth direction.
The growth seen from Figure 4.14(a) to (f) takes place within 24 min. It would be interesting to see whether this growth speed is limited by the low oxygen pressure present here or by other factors. Unfortunately, observing the formation in situ was so far only possible in pure CO and not when significant amounts of oxygen are present. We attribute this to a different interaction of the gases with the tip of the scanning tunneling microscope. Whereas the CO can surely adsorb on the platinum iridium tip it does not seem to influence the imaging too much. On the other hand, oxygen might oxidize the tip and roughen it which could explain a strongly diminished resolution observed here. Images taken in O_2 often show that multiple points on the tip tunnel at the same time.

4.5.4 Carbon Structures after CO Exposure

On clean as well as contaminated Au(111), structures form during CO exposure which are not present after exposure to the reaction mixture. The first of these structures is marked with white circles in Figures 4.5(b) and 4.11(b). It can be seen over the entire terrace suggesting that it is unrelated to the formation of the gold oxide islands. Taking a closer look in Figure 4.15, regular lines are visible in this structure. It strongly resembles the carbon film on Pt(111) observed by Starr et al. (Figure 1(c) in Ref. [194]). We measure the line-to-line distance in their image as 0.33 nm, which is the graphite layer distance [195] and thus supports the interpretation of Starr et al. that their film consists of small graphite domains. In contrast, the line-to-line distance in our structure is (0.51 $\pm$ 0.02) nm, as concluded from averaging over multiple images. The height with respect to the gold substrate appears between 0.06 nm and 0.15 nm in the STM. As can be seen in the height profile in Figure 4.15, multiple layers of the smallest height of 0.06 nm seem to be present. The line-to-line distance we measure agrees with the line-to-line distance of diamond(100)-2x1 [196,197]. The measured layer thickness is somewhat lower than the step height of diamond(100)-2x1, which is 0.089 nm as calculated from the crystal structure [198] and observed in Ref. [196]. However, the

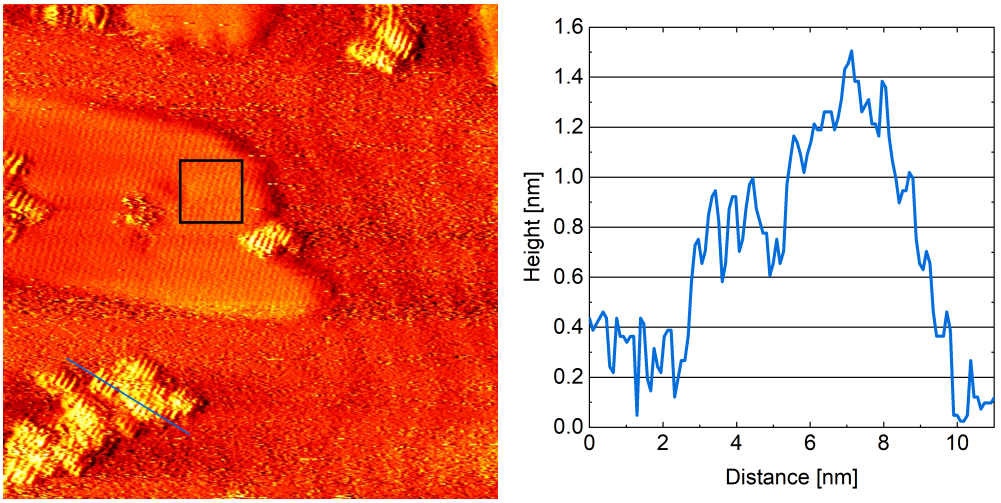

Figure 4.15: 40 nm x 40 nm STM image of contaminated Au(111) after exposure to 0.2 bar CO for 1 h. The image is taken in UHV at room temperature with − 1 V and 50 pA. For better visibility of all structures the image was merged with its derivative. A black square of 5 nm x 5 nm marks a gold oxide island. Another structure formed appears yellow. A height profile through one of these is drawn on the right and is indicated by the blue line in the STM image.

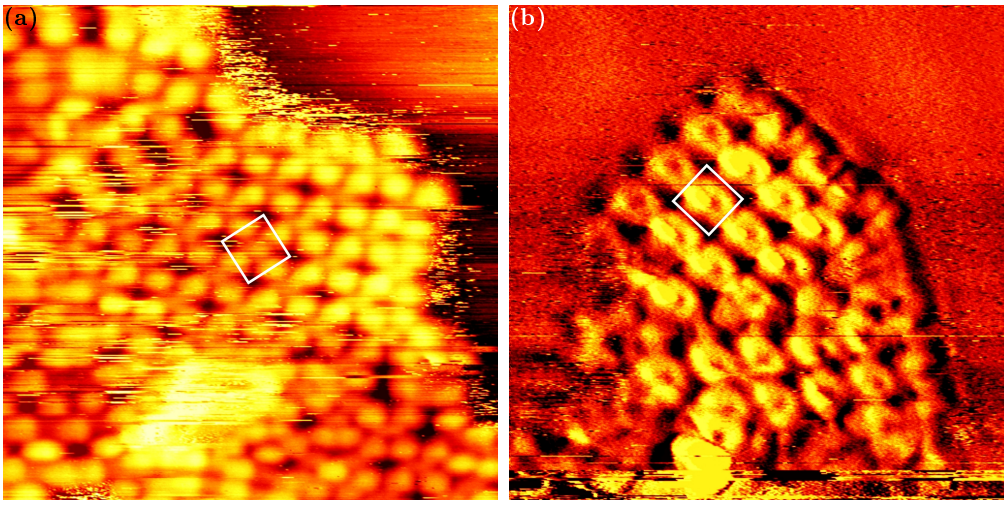

Figure 4.16: 10 nm x 10 nm STM images of the second structure observed after CO exposure showing the two different appearances in (a) and (b). The unit cell is marked with a white square. The images are taken in UHV at room temperature with (a) − 1 V and (b) − 1.5 V, and 50 pA. For better visibility of the details inside the unit cell the image in (b) is merged with its derivative in a ratio of 4:1.

height could be underestimated in our STM, especially as the structure is likely not completely conductive [199]. There is some evidence that on Au(111) diamond should rather grow as the diamond(111) orientation [200,201]. On the other hand, theory suggests that diamond(111) does not interact strongly with gold [202], which could allow for other orientations to grow as well. Overall, we have to conclude that further investigation is needed to unambiguously identify this structure.
As to the origin of the carbon, direct dissociation of adsorbed CO can be excluded as the atomic oxygen would form gold oxide next to every carbon structure. However, dissociation via another route which does not leave atomic oxygen on the surface cannot be excluded. Additionally, the hydrocarbon background from the CO bottle could cause the deposition of carbon. A clear conclusion cannot be reached without further research into the formation of the structure, which could be done by intentionally exposing the clean Au(111) surface to different sources of carbon.
The second structure observed is shown in Figure 4.16. It can appear in two different shapes in the STM (shown in (a) and (b)), which have the same squared unit cell with a length of (0.99 ± 0.02) nm in both directions (see white squares in Figure 4.16), as concluded from averaging over multiple images. This structure is only found connected to a step edge, suggesting that it is formed via a different mechanism than the first structure. However, an adsorption structure of CO itself can be excluded as it should not be stable in UHV at room temperature for several hours [176–179]. No similar adsorption structures on Au(111) could be found in the literature. Westenfelder at al. [203] have grown gold carbide layers on a graphene sheet decorated with gold nanoparticles. They exhibit an fcc(100) structure in which the quadratic unit cell has a length of (0.335 ± 0.01) nm in both directions. Taking the standard deviations into account the length of the unit cell measured here is in agreement with three times the length of this gold carbide unit cell. Westenfelder et al. imaged the carbide layers with transmission electron microscopy, in which the carbon atoms might not be visible between the gold atoms. As both gold and carbon are visible in STM, the larger unit cell measured here could be due to variations in the location of the carbon atoms. However, this would disagree with the three possible structures that Westenfelder at al. propose for the gold carbide. As it preferentially grows on the Au(111) facet of gold nanoparticles, the carbide would likely be stable on a Au(111) single crystal surface. However, it is formed at temperatures close to the melting point of gold in Ref. [203] such that it is unclear whether a formation via the same mechanism would be possible at room temperature. Overall, more investigation is needed for a clear identification of the structure observed here. Specifically, the dependence on bias voltage in STM and the elemental composition in spectroscopy should be studied. Observing the formation in CO at higher temperatures as well as studying the thermal stability of the structure

in UHV would allow for a more conclusive comparison to the gold carbide observed in Ref. [203].
As both structures observed here do not form in the same partial pressure of CO when O_2 is present as well, the oxygen is either able to suppress the formation or remove the structure after formation. Further experiments are needed to clarify this. Additionally, the water content in the CO used here could play a role, which should be investigated by using dried CO.